

Research Paper

Thermal performance of a radiatively cooled system for quantum optomechanical experiments in space



André Pilan Zanoni^{a,1,*}, Johannes Burkhardt^a, Ulrich Johann^a, Markus Aspelmeyer^b, Rainer Kaltenbaek^{b,*}, Gerald Hechenblaikner^{a,2}

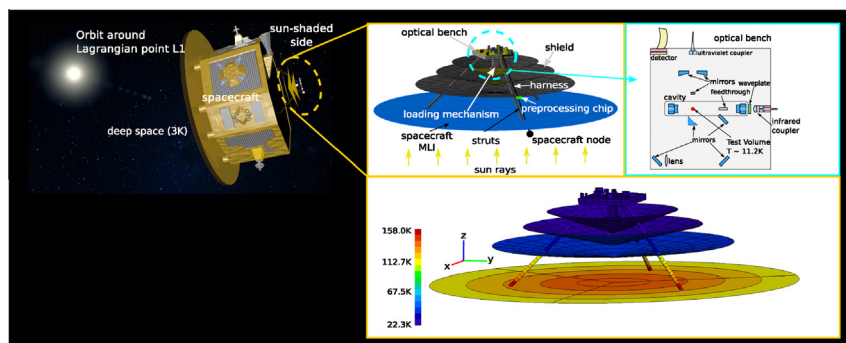
^a Airbus Defence and Space GmbH, Claude-Dornier-Straße, 88090 Immenstaad, Germany

^b Vienna Center of Quantum Science and Technology, Faculty of Physics, University of Vienna, Boltzmannngasse 5, 1090 Vienna, Austria

HIGHLIGHTS

- We improved performance and design aspects of a radiatively cooled instrument.
- A heat-flow analysis showed near optimal performance of the shield design.
- A simple modification to imaging optics allowed further improvements.
- We studied the thermal behavior for different orbital cases.
- A transfer-function analysis showed strong attenuation of thermal variations.

GRAPHICAL ABSTRACT



ARTICLE INFO

Article history:

Received 21 August 2015

Revised 16 June 2016

Accepted 17 June 2016

Available online 18 June 2016

Keywords:

Cryogenic instrument

Space missions

Optomechanics

System engineering

Quantum physics

MAQRO

ABSTRACT

Passive cooling of scientific instruments via thermal radiation to deep space offers many advantages over active cooling in terms of mission cost, lifetime and the achievable quality of vacuum and microgravity. Motivated by the mission proposal MAQRO to test the foundations of quantum physics harnessing a deep-space environment, we investigate the performance of a radiatively cooled instrument, where the environment of a test particle in a quantum superposition has to be cooled to less than 20 K. We perform a heat-transfer analysis between the instrument components and a transfer-function analysis on thermal oscillations induced by the spacecraft interior and dissipative sources. The thermal behavior of the instrument is discussed for an orbit around a Lagrangian point and for a highly elliptical Earth orbit. Finally, we investigate possible design improvements. These include a mirror-based design of the imaging system on the optical bench (OB) and an extension of the heat shields.

© 2016 The Authors. Published by Elsevier Ltd. This is an open access article under the CC BY-NC-ND license (<http://creativecommons.org/licenses/by-nc-nd/4.0/>).

Material properties between 20 K and 300 K

Aluminized coating [1] $\alpha = 0.05$, $\varepsilon = 0.15$

Aluminum Al 5083 [2,3] $\rho = 2800$,

$k = 17.21 - 119.3 \text{ W}/(\text{m} \cdot \text{K})$, $c = 8.90 - 902.0 \text{ J}/(\text{kg} \cdot \text{K})$

Black painting [1] $\alpha = 0.90$, $\varepsilon = 0.90$

Foam [1] $\rho = 40$, $k = 0.021 \text{ W}/(\text{m} \cdot \text{K})$, $c = 1300 \text{ J}/(\text{kg} \cdot \text{K})$

GFRP [4,5] $\rho = 2100$, $k = 0.14 - 0.70 \text{ W}/(\text{m} \cdot \text{K})$,

$c = 2.0 - 850 \text{ J}/(\text{kg} \cdot \text{K})$

* Corresponding authors.

E-mail addresses: andre.pilan.zanoni@cern.ch (A. Pilan Zanoni), johannes.burkhardt@airbus.com (J. Burkhardt), ulrich.johann@airbus.com (U. Johann), markus.aspelmeyer@univie.ac.at (M. Aspelmeyer), rainer.kaltenbaek@univie.ac.at (R. Kaltenbaek), ghechenb@eso.org (G. Hechenblaikner).

¹ Present address: CERN-European Organization for Nuclear Research, EN-STI-TCD, Geneva 23, Switzerland.

² Present address: European Southern Observatory (ESO), Karl-Schwarzschild-Straße 2, 85748 Garching bei Muenchen, Germany.

Nomenclature

Latin letters

\dot{Q}	rate of heat flow [W]
A_i	radiating surface of a node i [m ²]
c	specific heat capacity [J/(kg·K)]
d_i	distance between the barycenter of a node and the interface to an adjacent node [m]
F_{ij}	view factor of a node j seen from a node i [-]
k	thermal conductivity [W/(m·K)]
m	node mass [kg]
S	cross section between two nodes [m ²]
T	temperature [K or °C]
t	time [s]
CTE	coefficient of thermal expansion [K ⁻¹]
HTC	heat transfer coefficient [W/(m ² ·K)]

Greek letters

α	solar absorptivity [-]
ν	resonance frequency in the cavity [Hz]
σ	Stefan-Boltzmann constant [$5.67 \times 10^{-8} \text{Wm}^{-2}\text{K}^{-4}$]
ε	infrared emissivity [-]

Abbreviations

CCD	charge-coupled device
EOL	end of life
ESA	European space agency
FT	feed through
GFRP	glass-fiber reinforced plastic
GMM	geometric mathematical model
IR	infrared
LM	loading mechanism
MLI	multi-layer insulation
OB	optical bench
TMM	thermal mathematical model
TV	test volume
UV	ultraviolet

Units

AU	astronomical unit: $1 \text{ AU} = 1.496 \times 10^{11} \text{ m}$
----	--------------------------------------------------------------------

Gold coating [1] $\alpha = 0.02$, $\varepsilon = 0.06$
 Kapton[®] MLI [1] HTC = $0.021\text{--}0.072 \text{ W/m}^2 \text{ K}$,
 $\alpha = 0.92$, $\varepsilon = 0.46$
 SiC [1,6,7] $\rho = 3200$, $k = 35.0\text{--}180.0 \text{ W/(m} \cdot \text{K)}$,
 $c = 0.7\text{--}665.1 \text{ J/(kg} \cdot \text{K)}$, $\alpha = 0.69$, $\varepsilon = 0.85$
 Titanium Ti6Al4V [8–12] $\rho = 4430$,
 $k = 1.50\text{--}7.70 \text{ W/(m} \cdot \text{K)}$, $c = 8.20\text{--}538.6 \text{ J/(kg} \cdot \text{K)}$
 Wire steel AISI 301 [13,14] $\rho = 7900$, $k = 0.70\text{--}15.0 \text{ W/(m} \cdot \text{K)}$,
 $c = 67.04\text{--}460.0 \text{ J/(kg} \cdot \text{K)}$
 ZERODUR[®] [1,15] $\rho = 2530 \text{ kg/m}^3$, $k = 0.12\text{--}1.46 \text{ W/(m} \cdot \text{K)}$,
 $c = 25.13\text{--}800 \text{ J/(kg} \cdot \text{K)}$, CTE = $-0.63 \times 10^{-6} \text{ K}^{-1}$, $\alpha = 0.80$, $\varepsilon = 0.30$

1. Introduction

To observe quantum effects with macroscopic optomechanical systems, they need to be well isolated [16,17]. Mechanical support can pose limits due to thermal and vibrational coupling to the environment. Even utilizing optically trapped test particles, one may have to switch off the trap and observe quantum effects in free fall [18,19].

While Earth-bound experiments are limited to short free-fall times, deep space offers favorable conditions like microgravity, long free-fall times, outstanding vacuum quality (ca. 10^{-15} mbar) and low temperatures (ca. 2.7 K). Optimally harnessing deep space, however, requires a thermal design to shield quantum systems from heat loads like the spacecraft and nearby celestial bodies.

An alternative is active cooling [20], but it requires cryogenic helium tanks and pumps, which add additional mission control variables and extra mass to be launched to space. Helium supply limits the mission lifetime, and helium may interact with test particles, leading to decoherence.

These limitations can be overcome by passive cooling. Concepts for passive cooling were suggested in [21], where shields blocked sun radiation from reaching telescope mirrors. Ref. [22] achieved a temperature of 20 K. Modern space missions like James Webb [23], Gaia [24,25] and Planck [26] use similar systems. Thermal shields can also act as wake shields [27] and protect against solar wind and spacecraft outgassing [19].

This approach was first suggested for quantum experiments in the mission proposal MAQRO [19]. Later, it was investigated in more detail to achieve the low environment temperature (20 K) and excellent vacuum ($\sim 10^{-15}$ mbar) [28,29] required to observe quantum interference of massive particles to test the foundations of physics.

A first thermal-shield design [29] focused on determining the lowest temperature achievable via passive cooling in space. Fig. 1 shows features of this design. A number of three shields was found to be a good choice because more shields increase the instrument's complexity without significant benefit [29]. We determined the optimal distances between the shields and their opening angles by first assuming a fixed ratio between the various distances and angles and then optimizing the opening angle and the distance of the outermost shield with respect to the temperature of the "test volume" (TV), the immediate environment around the test particle. We confirmed that our assumptions were optimal by varying the opening angles and distances of the shields with respect to each other and the effect on the TV temperature. Including anticipated optical and electrical dissipation on the OB and heat transfer from the spacecraft via conduction and radiation, we achieved a TV temperature of 16.3 K. Several performance issues like heat-transfer dynamics and orbital cases remained to be investigated.

Here, we improve the shield design for achieving even lower temperatures. We conducted heat-flow and transfer-function analyses. The latter allowed evaluating the attenuation of thermal fluctuations from their origin to where the experiment is performed. Moreover, we improved the OB design by replacing refractive with reflective optics.

2. Modeling approach

We model the scientific instrument using ESATAN-TMS r4 [31]. The radiative couplings between instrument surface nodes are calculated using a geometric mathematical model (GMM) and Monte-Carlo ray tracing. These values are fed into a thermal mathematical model (TMM). Further inputs for solving the energy equation are conductive couplings between instrument nodes, internal and external heat loads, boundary conditions and parameters for numerical processing. The TMM uses the lumped-parameter for-

mulation, where all properties of a node are concentrated in its barycenter.

2.1. The geometric and thermal mathematical models

Fig. 1 illustrates the GMM for MAQRO [19,28,29]. The TV is modeled as a black body with $\alpha = \epsilon = 1$ and zero specific heat capacity ($c = 0$) representing the empty volume in direct vicinity of the test particle [29].

The central element on the OB is a high-finesse optical cavity formed by two spherical mirrors. Using multiple IR cavity modes (1064 nm), test particles are trapped and cooled [32]. For the present study, we assumed the presence of several reflective optical elements for UV light to prepare macroscopic superpositions [19,33].

Excepting optical dissipation of the cavity mirrors, our thermal simulations assume all optical fields to be turned off. This is a worst-case estimation because other strong sources of dissipation (e.g., detector, preprocessing chip) can often be turned off or down (in frame rate) [30].

We assumed the OB and the structural elements of the LM to be made of ZERODUR® as in LISA Pathfinder [34]. The top surface of the OB is gold coated to minimize radiative heat transfer to the TV [29]. We assume optical elements to consist of fused silica and to be hydroxide-catalysis bonded to the OB [35]. Due to the polymerization process described in [35] we calculated the GL between the optical components and the OB according to Eq. (1) assuming perfect contacts.

Three struts support the OB and connect it to the spacecraft. These are hollow GFRP tubes filled with polyurethane foam to avoid radiative heat exchange between the inner surfaces of the strut [29]. Titanium fittings (Ti6Al4V) connect struts and shields (see Fig. 1). A set of shields prevents spacecraft heat radiation from

reaching the bench [21]. Each comprises an aluminum plate (Al 5083) with the bottom covered with a 20-layer MLI (Fig. 1).

The boundary nodes are deep space (3 K) and the internal spacecraft temperature (20 °C), a typical mean value in payload operation (e.g., [36]). Harness, optical fibers and the preprocessing chip were not geometrically modeled. Their small emitting areas render their radiative influence on the OB negligible [29].

We calculate the radiative coupling $GR(i,j)$ and the view factors F_{ij} from the geometric surface model for each pair of surface nodes via Monte-Carlo simulation in ESATAN-TMS r4 [31]. It statistically evaluates the emission and the propagation of electromagnetic rays from and between surface elements.

We sample a fixed quantity of 10,000 rays from each surface node, compare with [37,38]. This quantity was increased to 100,000 rays for pairs including the TV. We calculated $GR = 7.4 \times 10^{-5} \text{ m}^2$ for the radiative coupling between the TV and deep space.

We also use Monte-Carlo ray tracing for the orbital cases to evaluate external heat loads radiated on all the instrument's external surfaces like solar, albedo and Earth infrared heat [31].

2.2. The thermal mathematical model and the energy equation

Conductive couplings $GL(i,j)$ between nodes were calculated using Eq. (1).

$$GL(i,j) = (GL_i^{-1} + GL_j^{-1})^{-1} = \left[\left(\frac{k_i(T)S_{ij}}{d_i} \right)^{-1} + \left(\frac{k_j(T)S_{ij}}{d_j} \right)^{-1} \right]^{-1} \quad (1)$$

The preprocessing chip [30,39] is assumed to be attached below the first shield, preventing its dissipation from directly affecting the OB. The chip is assumed to fit between shield and MLI without direct contact to the latter. The harness connecting detector chip,

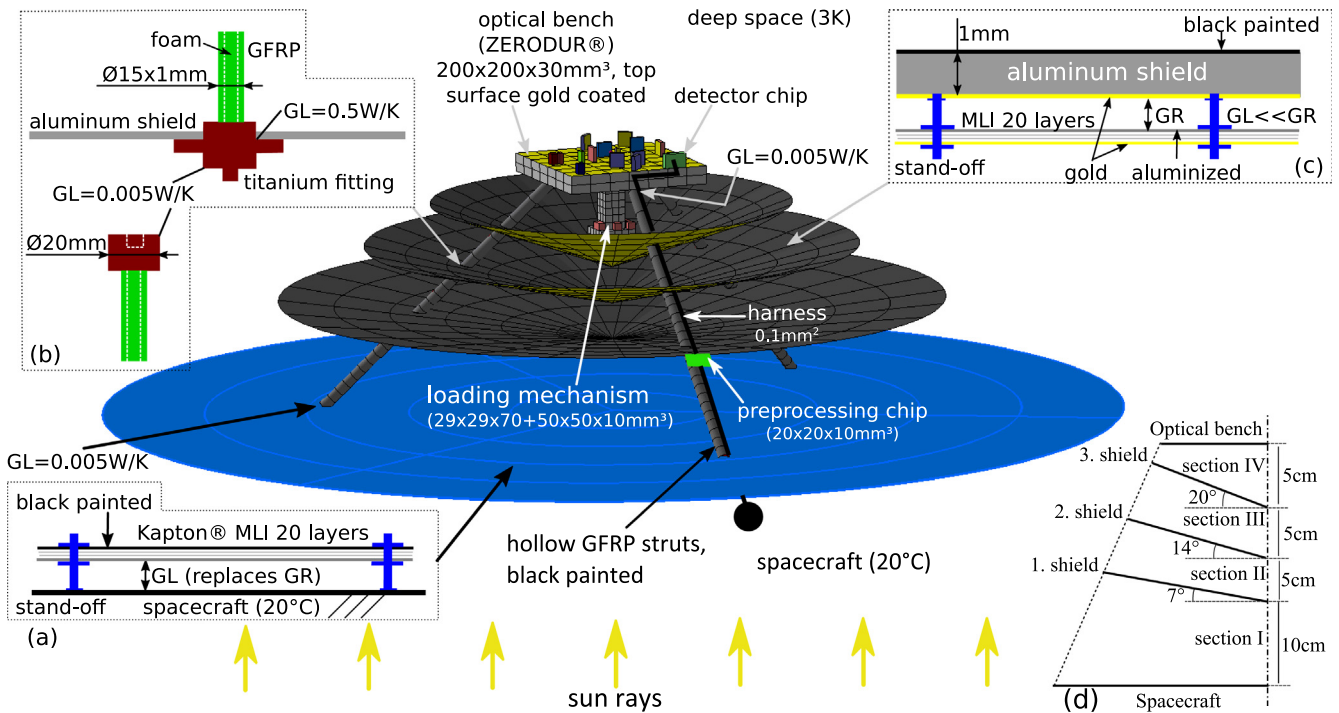


Fig. 1. Schematic representation of the geometric mathematical model of the MAQRO instrument. The bottom disc represents the spacecraft MLI ($GL = A \times HTC$) with an outer layer of black Kapton (a). MAQRO uses dielectric nanospheres as test particles, which are supplied to the cavity from a “Loading mechanism” (LM). A CMOS “detector chip” [30] detects scattered light on the optical bench (OB). (b) Coupling assumed between struts and shields [29]: $GL = (GL_{Ti}^{-1} + (GL_{GFRP} + GL_{foam})^{-1})^{-1}$, (c) shield MLI ($GR = A / (\epsilon_{Au}^{-1} + \epsilon_{Al}^{-1} - 1)$). The aluminum plates are flat, 1 mm thick, black painted on top and gold coated below. No stiffeners are used. The MLI (each layer $\sim 12 \mu\text{m}$ thick) is aluminumized on top and gold coated below. (d) Axis-symmetric shielding structure. The opening angles and relative distances were derived in [29].

preprocessing chip and spacecraft (see Fig. 1) is assumed to consist of steel [13,14]. The thermal properties of the chips are assumed to be like quartz glass.

Based on [29], we neglected optical fibers in our model. Spacecraft, shields and OB are assumed to be connected to the struts using titanium fittings (see Fig. 1(b)). These are included as constant conductive couplings [29].

We evaluate the heat-flow rate between nodes using the equations for radiative $\dot{Q}_{R,ij}$ and conductive heat flow $\dot{Q}_{L,ij}$:

$$\dot{Q}_{R,ij} = GR(i,j)\sigma(T_i^4 - T_j^4) \quad (2)$$

$$\dot{Q}_{L,ij} = GL(i,j)(T_i - T_j) \quad (3)$$

For each node i , we evaluate the energy equation using Eq. (4) (see [31,40]):

$$\sum_i (\dot{Q}_{R,i} + \dot{Q}_{L,i} + \dot{Q}_{S,i} + \dot{Q}_{E,i}) = m_i c_i \frac{\partial T_i(t)}{\partial t} \quad (4)$$

Indices R, L and I refer to radiative, conductive and dissipative heat. S refers to solar heat, E to Earth albedo and infrared radiation.

Dissipation sources considered in the TMM are: preprocessing chip (10.0 mW), detector chip (1.0 mW) and cavity mirrors (0.2 mW) [29]. We assumed these sources of dissipation to be active continuously – a worst-case scenario because the dissipation can be reduced during free-fall times of the test particle [19].

The energy equation is evaluated for each model node and treated numerically (see [31]). Iterative and inverse matrix solvers are used for the steady state. As a plausibility check, we compared the temperature predicted by these methods for the TV. The difference was ≤ 0.1 K. For the transient cases, we used the Crank-Nicolson method [41] and the backward-differentiation method based on the Gear formalism [42]. The results of these methods differed by less than 2 K.

2.3. Transfer-function analysis

The solar radiation varies along an HEO orbit, potentially leading to oscillations of the spacecraft temperature. We investigate

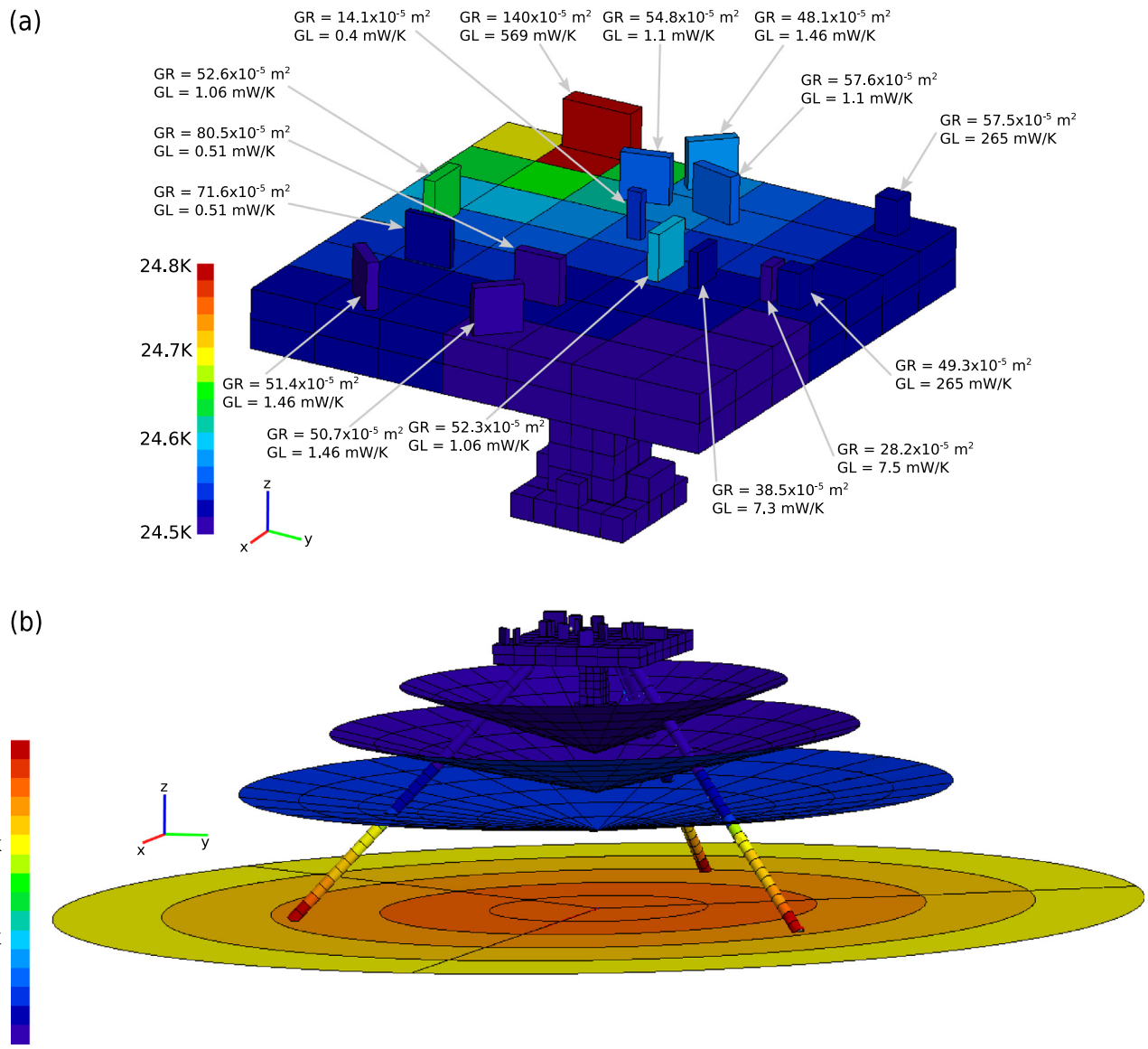


Fig. 2. Temperature map of the MAQRO instrument. (a) Temperature distribution of the optical bench (OB) as well as conductive and radiative couplings of the optical elements to the OB (GL) and to space (GR), respectively. (b) Temperature map of the thermal shields, the struts and the spacecraft MLI.

the influence of such oscillations on the instrument temperature using a transfer-function analysis in steady state. For that purpose, the energy equation is linearized and Laplace transformed from the time to the frequency domain [43]. We start from a steady-state temperature distribution and then analyze how spacecraft temperature variations affect the temperature of instrument components. Due to the linearization, only small spacecraft-temperature variations (≤ 5 K) can be considered [43]. This “gain” is calculated using TransFAST [44].

3. Results and discussion

In Figs. 2 and 3, we show a temperature map for all parts of the MAQRO instrument outside the spacecraft, the radial temperature distribution on the shields and the temperature distribution along a strut varying with the distance from the spacecraft for different mesh grids.

The analysis showed steady-state temperatures of ~ 13.9 K and ~ 24.7 K for the TV and OB. Reducing numerical averaging effects through a better mesh grid for the struts led to a ~ 2.4 K improvement compared to earlier results [29]. Based on the margin philosophy of Ref. [45], we estimate an uncertainty of ± 4 K for the temperature of the test volume. Figs. 2 and 3 show the temperature distribution for the shields and the OB to be virtually uniform.

3.1. Heat-flow analysis

We analyzed the heat flow in steady state to quantify the heat transfer between instrument components and to better assess the temperature results, see Fig. 4.

The heat flow results from the temperature difference between spacecraft (20°C) and deep space (3 K) and from the dissipation sources represented as red arrows. We divide these dissipation sources into the preprocessing chip and the OB (detector chip, cavity mirrors).

The dominant part of the spacecraft’s heat energy radiates directly to deep space from the spacecraft MLI (9785 mW). Smaller amounts radiate to deep space from the shields. This plays an important role for passive cooling because, in addition to preventing energy from reaching the OB, the shields act as radiators receiving energy conductively via the struts and radiating it to space. Similarly, only a small part of the 10 mW dissipation of the preprocessing chip flows through the harness. Most is conducted to the first shield and radiated to space. This assumes an idealized direct contact between the preprocessing chip and the first shield (using Eq. (1)), leading to a conductive coupling of around 2.8 W/K. For comparison, the coupling between harness and preprocessing chip is 3.3×10^{-5} W/K.

A sensitivity analysis showed that the temperature of the TV increases to ~ 20 K if the dissipation of the detector chip increases from 1 mW to 12 mW.

The dissipation of electronic and optical elements on the optical bench results in a lower temperature (22.4 K) of the third shield compared to the OB (24.7 K). Although little radiative heat from the other shields reaches the third one, this shield is important for cooling the OB by receiving part of the heat from the bench and radiating it to space. Removal of the third shield would cause a considerable increase of the TV temperature [29].

The first strut section removes a great part of the energy radiatively to deep space. The amount of heat radiated from the struts diminishes along the struts because of the thermal attenuation induced by the shields. Due to dissipation on the OB, the fourth section radiates slightly more heat than the third.

Fig. 4 illustrates that the shield configuration performs well for passively cooling the OB because the heat flow on the path from the spacecraft to the OB is strongly attenuated. Adding more shields is unnecessary because it would significantly increase the instrument complexity while only yielding a slight increase in that attenuation [29].

Finally, the heat flow in the instrument is consistent with the temperatures shown in Fig. 3. For instance, the low temperatures

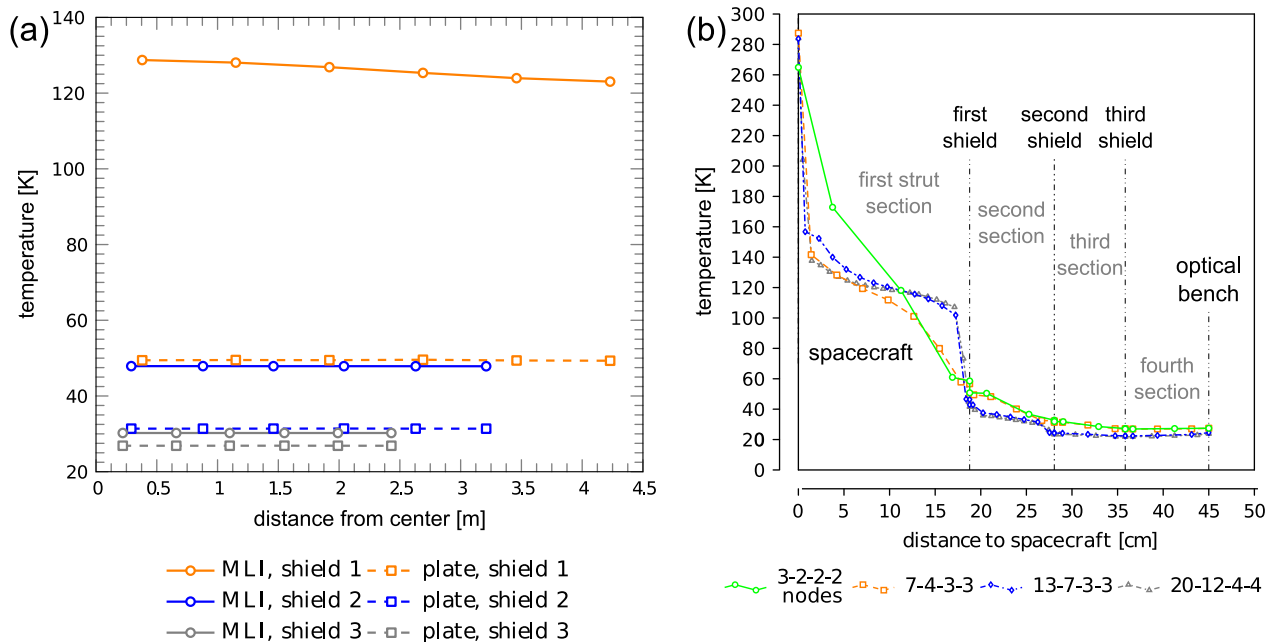


Fig. 3. (a) Radial temperature distribution of the shields. The difference between the temperature in the center and the border of the first shield is about 7 K, whereas the temperature of the other shields is radially virtually constant. (b) Temperature distribution along an individual strut for three different mesh grids. A very high temperature difference between beginning and end of the struts is observed. Note that the best mesh was achieved by the configuration 13-7-3-3 (13 axial nodes for the first strut section, 7 for the second section, and 3 for the third and fourth sections each). Using finer meshes is unnecessary because it results in the same temperature distribution for regions close to the OB.

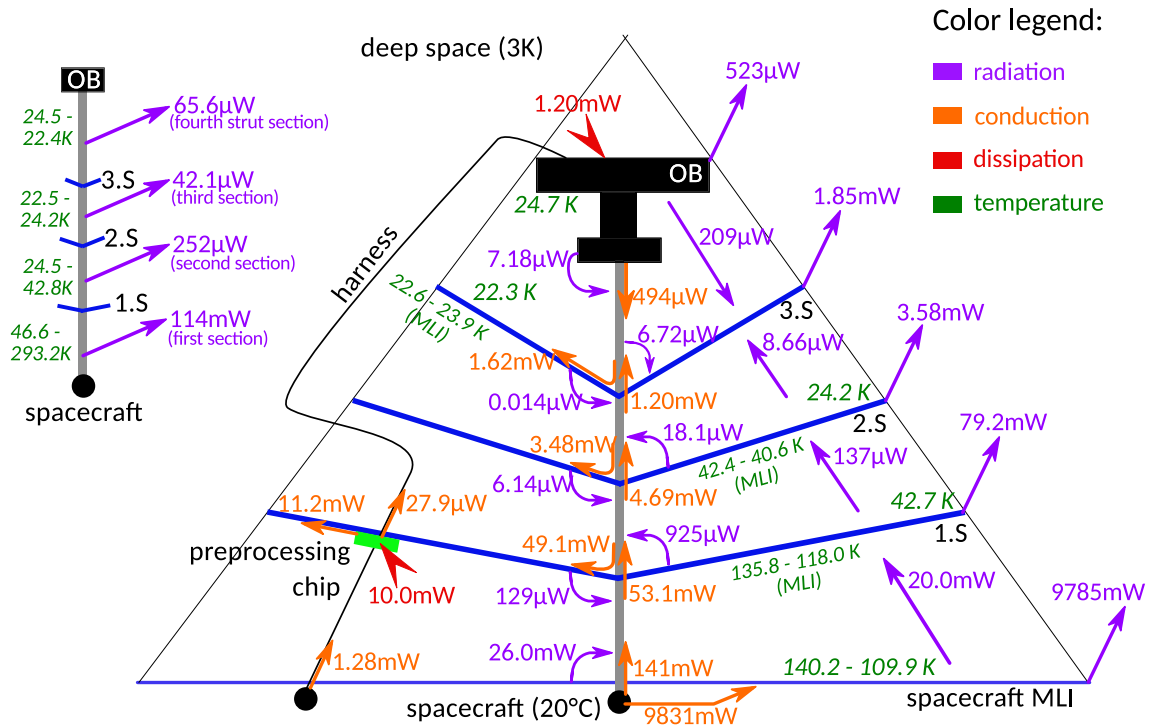


Fig. 4. Schematic heat-flow diagram of the entire instrument. The figure shows the three shields (1.S, 2.S and 3.S), the OB and the spacecraft MLI. For simplicity, the struts are represented as a single gray tube and the radiative flow of each strut section to space is detailed in an inset on the left-hand side. Thin black lines form a triangle illustrating the line of sight between spacecraft and OB. The OB must be inside that triangle to avoid direct irradiation from the spacecraft. Radiative heat flow is represented in purple, conductive heat flow in orange. The temperature values are shown in green. The harness is represented as a loose black line.

obtained for the TV and the OB result from the amount of heat circulating in the bench being much smaller than that circulating in the shields and struts.

3.2. Transfer-function analysis

Using a transfer-function analysis, we investigated the effect of spacecraft temperature oscillations on the instrument temperature. We considered temperature oscillations with frequencies in the range of $10^{-6} - 10^{-1}$ Hz, corresponding to oscillation periods between 10 s and 11.6 days. These periods cover the experimental time scales in MAQRO (time per measurement, time period where the OB temperature is <20 K during an HEO). Changes of the OB temperature have to be slow compared to the duration of a single measurement in MAQRO (100 s) [19]. A measurement series can last many days. Fig. 5 shows the gains for various instrument components, i.e., the differential temperature at the output (instrument component) divided by the differential temperature at the input (e.g., spacecraft temperature fluctuations). Thermal disturbances are transferred on a much slower time scale compared to, e.g., electrical oscillations. Consequently, the inertia of thermal fluctuations, especially at low frequencies, lead to larger thermal gains.

Fig. 6 shows a detailed analysis of gains for a frequency of 10^{-6} Hz. We chose this analysis because it induces the largest gains. The gain for each strut section corresponds to the average of the three struts belonging to the same section.

Instrument components conductively linked to the spacecraft, like the first section of the struts and the first section of the harness, have the highest gains. Components radiatively coupled to the spacecraft have smaller gains. Components directly connected to the source of oscillation, like the MLIs of the spacecraft and of the first shield, are strongly influenced by spacecraft temperature variations, resulting in higher gains compared to far-off components.

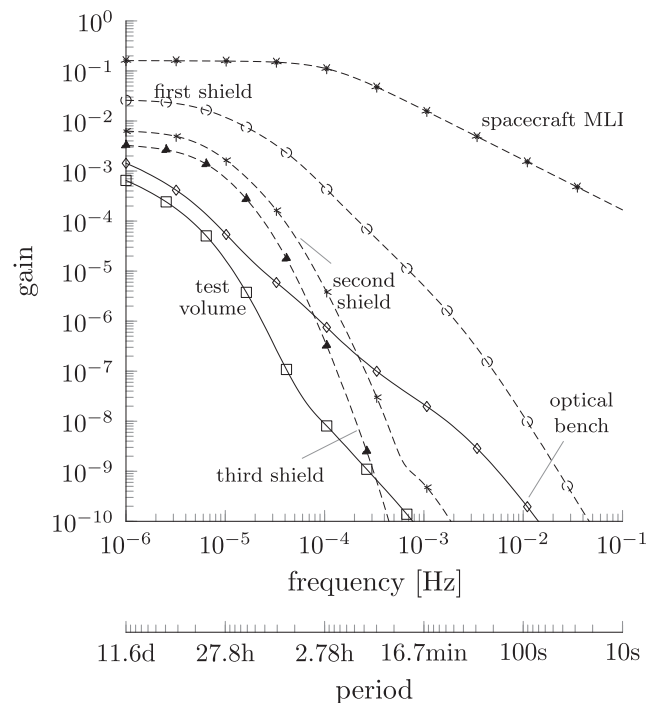


Fig. 5. Results of the transfer-function analysis, plotted on a logarithmic scale for each of the major instrument components, with the spacecraft temperature at 20°C as the single input.

Fig. 6(a) shows that spacecraft temperature oscillations have little effect on the OB temperature. The gain is 1.4×10^{-3} – a change of 5 K for the spacecraft over 11.6 days only results in a <0.01 K change at the OB. But even small variations could influence the

fractional frequency instability of the MAQRO cavity. We define this frequency instability as $|\Delta\nu/\nu_{\text{Res}}| = |\Delta L/L|$. Let us assume a coefficient of thermal expansion (CTE) for ZERODUR® of $-0.63 \times 10^{-6} \text{ K}^{-1}$ at 30 K, a cavity length $L \approx 100 \text{ mm}$ and an attenuation by a factor 5×10^{-10} for temperature fluctuations of 5 K over 100 s. Then the relative change in cavity length will be $|\Delta L/L| \approx 1.6 \times 10^{-16}$. This is comparable to the best fractional frequency instabilities achievable in ground-based cavities today [46–48].

Because we linearized the radiative terms in solving the energy equation, the results for temperature gains are only accurate for small variations (see Section 2.3). However, a sensitivity analysis in steady state with a physically representative nonlinear thermal model showed that the temperatures of TV and OB remain small for a wide range of input temperatures. Even a temperature increase from 80 K to 373 K only induces a temperature increase from 22.8 K to 24.9 K for the OB and from 10.6 K to 11.6 K for the TV. This input temperature range is definitely not applicable to a real spacecraft – we only used it for a numerical sensitivity analysis.

We also investigated the effect of oscillations of dissipation in the preprocessing chip. These may, e.g., result from operating the CMOS detector at different frame rates [30,39]. The gains [in K/mW] are defined as the differential temperature at components divided by the differential power in the dissipation of the preprocessing chip (see Fig. 6(b)). Because electric components typically exhibit high oscillation frequencies, our investigation considering a very low frequency of 10^{-6} Hz represents a worst-case scenario for thermal oscillations.

The aluminum plate of the first shield and both harness sections show high gains due to their direct connection to the preprocessing chip via thermal conduction. The MLI of the first shield has low gain because it is not conductively coupled to the preprocessing chip, and the GR between them is negligible (see Section 2.2).

Because the preprocessing chip is mounted below the first shield near a strut, the gain of this strut is higher than that of others. The gains of the struts from the third section are similar because the dissipation of the preprocessing chip is less dominant there.

The gain for the OB is $\sim 8.5 \times 10^{-3} \text{ K/mW}$, resulting in a frequency instability of the optical cavity similarly low as for spacecraft temperature fluctuations.

3.3. Improving the thermal properties of the optical bench

We improved the OB of MAQRO with respect to the TV temperature by replacing lens F1 with a gold-coated parabolic mirror R1 and flat mirrors (see Fig. 7). The cavity mirrors are assumed to be bonded to ZERODUR® blocks with central holes, and these “spacers” are bonded to the OB. This allows maximum optical access to the nanosphere and is well suited for passive cooling of the TV.

Using reflective instead of refractive optics is advantageous because gold coating can minimize thermal radiation towards the TV. The mirror’s reflecting area is larger than the original lens to keep the numerical aperture constant. Comparing the two designs, we report an improvement from 13.9 K to 11.2 K for the TV temperature. Without coating, the temperature is higher (14.3 K) due to the larger area.

3.4. Orbital cases

We analyzed the transient thermal behavior of the instrument for two orbits: an orbit around the Sun-Earth Lagrangian point L2 and a quasi-stationary highly elliptical Earth orbit (HEO). For the first orbit, we perform a cool-down analysis of the instrument, whereas the analysis for the HEO aims at indicating operational constraints for an Earth orbit. The spacecraft temperature is assumed to be constant throughout the orbit.

3.4.1. Thermal-analysis results of the orbit around L2

For the L2 scenario, we assume the whole instrument to cool down by radiating to space starting at 20 °C. The orbit is assumed to be sun-oriented with the normal vector to the spacecraft surface pointing towards the sun. The instrument can be accommodated on the sun-shaded side of the spacecraft without direct solar radiation. At L2, the OB is also assumed to be shielded against direct Earth radiation.

The temperature of the instrument has a fourth-degree polynomial dependence on time. It drops quickly in the beginning and converges slowly towards steady state. This is consistent with deep space acting as the sole heat sink.

The first shield quickly reaches steady state (~ 3 days) because of its high steady-state temperature. The OB reaches steady state last due to its low steady-state temperature and high heat capacity. It takes ~ 24 days to reach a temperature $< 25 \text{ K}$. The TV tempera-

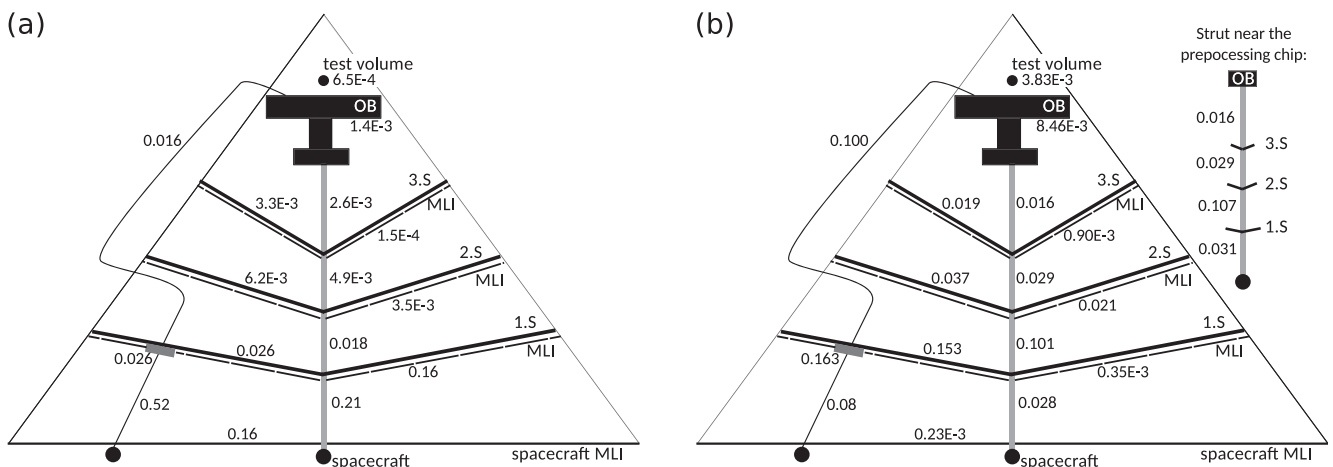


Fig. 6. (a) Calculated gains for different instrument components in [K/K] defined as the temperature response at the outputs divided by the input temperature oscillation. The spacecraft temperature at 20 °C is the single input and oscillates at a frequency of 10^{-6} Hz (period: 11.6 days). (b) Calculated gains for different instrument components in [K/mW] defined as the temperature response at the outputs divided by the input power oscillation. The 10 mW dissipation of the preprocessing chip is the single input and oscillates at a frequency of 10^{-6} Hz . A separate representation on the right-hand side shows the gains of the strut closest to the preprocessing chip.

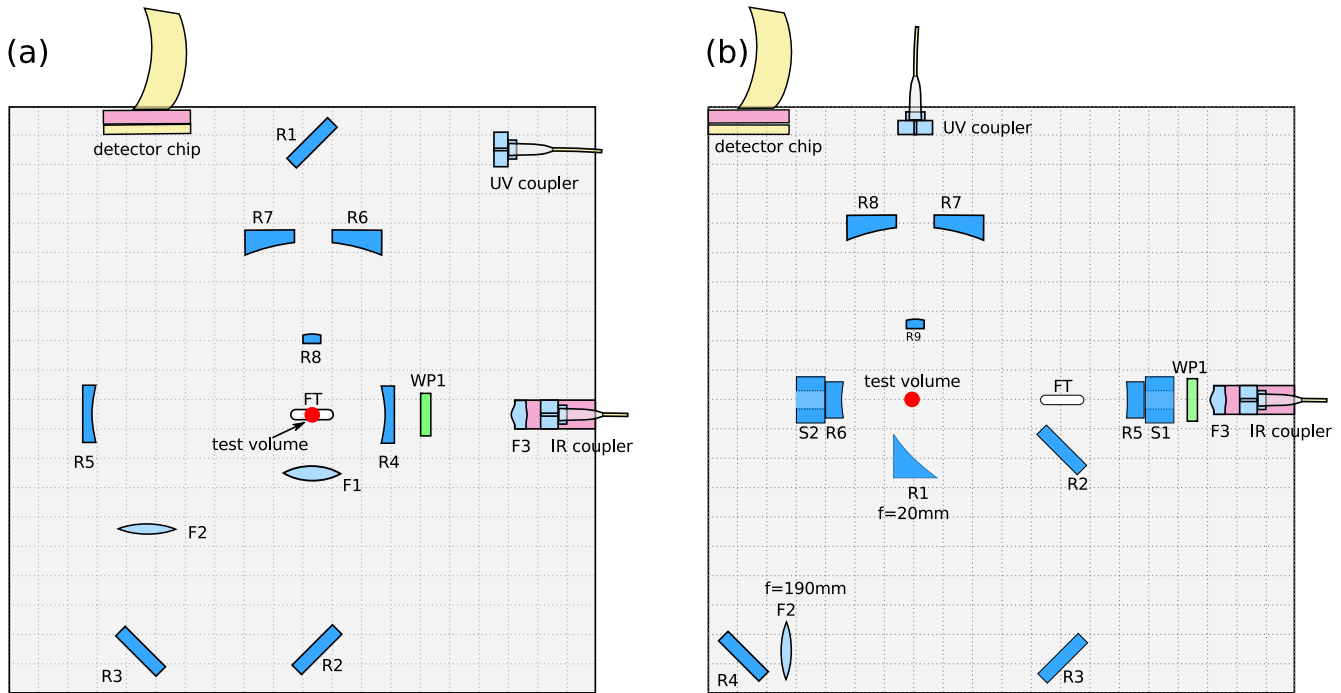


Fig. 7. (a) A preliminary design of the OB using refractive optics. (b) Improved design using reflective optics for reducing the temperature of the TV. The CMOS camera was developed for James Webb [30,39]. Legend: R ... mirrors, F ... focusing lenses, WP ... wave plate, S ... spacers, FT ... slit where the nanosphere is loaded into the cavity.

ture drops quickly in the beginning because of the high view factor to deep space and zero heat capacity. After ~8 days, it cools below 20 K and over another 16 days it drops by 8 K more. See Fig. 8(a).

3.4.2. Thermal-analysis results of the quasi-stationary highly elliptical orbit

The HEO parameters and the results are shown in Fig. 8(b). The criterion for a quasi-stationary HEO is fulfilled if all node temperatures periodically recur at a predetermined orbital position after successive cycles.

Each component's temperature is the average of the temperatures of its nodes. The instrument has a high (low) view factor to Earth at perigee (apogee). The solar heat incident was zero for all instrument nodes, confirming the sun orientation of the spacecraft.

The instrument temperature reaches its peak right after perigee and cools down while traveling towards apogee, where Earth's thermal influence significantly diminishes. The temperatures drop rapidly at first and then converge slowly towards steady state during the cooling phase before the spacecraft reaches the perigee again.

The temperature of the OB ranges between 26 K and 69 K. The maximum temperature change rate is ~ 10 K/day. Because of the OB's high heat capacity at low temperatures, its temperature change is smaller than for other instrument components.

It takes ~ 7 days for the TV to cool to < 20 K after passing through perigee. Its temperature reaches 12.2 K eleven days later. As the TV is modeled with zero heat capacity, its temperature increases from 12.2 K to 290 K within seven hours before reaching

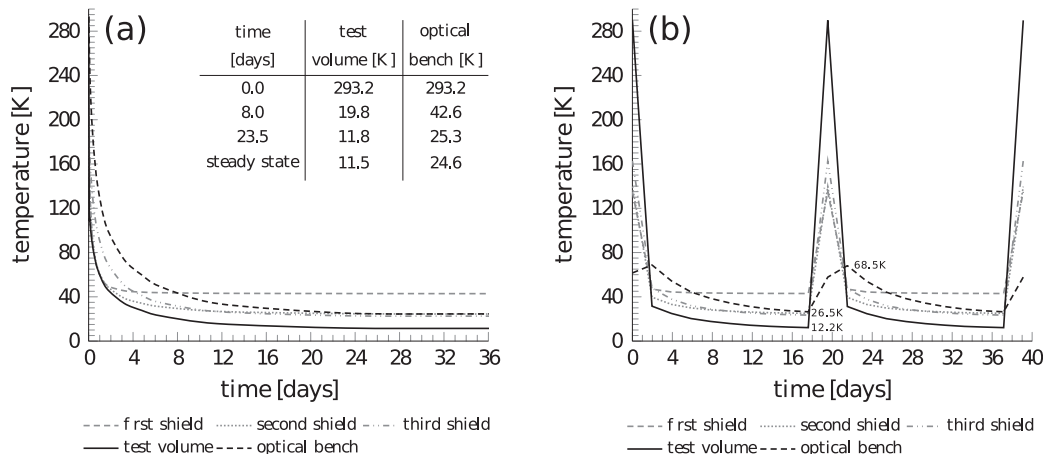


Fig. 8. Thermal results: (a) This scenario considers the spacecraft to be in an orbit around the Sun-Earth Lagrangian point L2 and a starting temperature of 20 °C. The distance between the spacecraft and the Earth is around 1.5×10^6 km. (b) This scenario considers a quasi-stationary highly elliptical orbit. Altitude at apogee: 600,000 km, altitude at perigee: 600 km, inclination: 63.4°, argument of periapsis: 0°, right ascension of the ascending node: 0°, orbital period: ~ 19.6 days. Average sun radiation flux of 1369 W/m² at 1 AU. Average Earth-albedo reflectance: 0.3. Uniform Earth infrared emissivity: 1 at 257 K. Calculated Earth heat flow on the OB: $\dot{Q}_{E,perigee} = 4.4$ W, $\dot{Q}_{E,apogee} = 0$ W.

the perigee. This also leads to the sudden temperature decrease after leaving the perigee.

3.4.3. Discussion of the orbital cases

In an HEO, the experiments must be interrupted each eleven days due to higher heat loads at perigee. In contrast, experiments can be performed without interruption around L2. While an HEO may offer flexibility in mission planning as the instrument could be flown on a satellite for Earth observation, the bench is periodically exposed to heat loads and temperature changes, which may cause misalignment of the bench components, high thermal stress [49] or even structural changes such as loss of bonding force between interfaces due to hysteresis effects caused by thermal cycling. In addition, the heat load from Earth is not uniformly distributed across the instrument, inducing an uneven temperature distribution.

3.4.4. Thermal results considering an SiC bench for the L2 scenario

At the cryogenic OB temperatures expected in MAQRO, ZERO-DUR® may not be the optimal material choice. At temperatures below 30 K, Silicon Carbide (SiC) has a significantly lower CTE [50]. For that reason, we performed a thermal analysis for an SiC OB in the case of an L2 orbit.

The results showed that the TV cooled down significantly faster using SiC. It reached a temperature < 20 K within 3 days (for ZERO-DUR®: 8 days). The OB reached 25 K in 5 days (for ZERO-DUR®: 24 days). This is due to the smaller heat capacity of SiC. Extrapolating these results to an HEO, one expects an extension of the time period during which the thermal requirements of MAQRO are fulfilled by ~ 5 days per orbital cycle.

Although SiC has a higher thermal conductivity than ZERO-DUR®, the steady-state temperatures of the TV for the ZERO-DUR® bench (11.4 K) and for the SiC bench (11.2 K) are nearly identical. This is consistent with the low heat reaching the OB (see Section 3.1).

3.5. Further concept improvements

Here, we discuss potential further design improvements for even lower TV and OB steady-state temperatures.

3.5.1. Configuration of the MLI on the shields

The heat-flow diagram in Fig. 4, shows the comparatively low radiative heat transfer on the third shield. Moreover, the oscillations of the spacecraft temperature and the variations of the preprocessing chip’s dissipation are strongly attenuated from the oscillation source to the MLI of the third shield (see Fig. 6). Therefore, we considered scenarios where the MLI was removed from one or more shields.

We observed that the MLI on the third shield has little influence on the steady-state temperatures of TV and OB. While the shield design can be simplified by removing that MLI, the aluminum plate of the third shield is essential for radiating heat to space, and because it acts as a heat sink for the OB (see Fig. 4).

Although removing the MLI from the second shield only results in slight changes in the TV and OB temperatures (≤ 0.2 K), one should retain this MLI because it has higher gain with respect to variations in the dissipation of the preprocessing chip (0.021 K/mW) than the MLI on the third shield (0.90×10^{-3} K/mW).

Due to the comparatively high heat flow on the MLI of the first shield, its removal would cause a significant change in the TV and OB temperatures by ~ 2.9 K. This renders the MLI of the first shield essential for passive cooling.

Table 1

Thermal results of the instrument with elongated shields. The choice of outer MLI layer (gold vs. black Kapton) strongly influences the MLI temperature, showing a difference of 150 K. Because $\alpha/\epsilon_{\text{Gold}} \approx 3.00$ and $\alpha/\epsilon_{\text{Kapton(EOL)}} \approx 0.75$, the gold layer absorbs more sun radiation than it can emit through infrared light. To avoid thermal degradation, the outer MLI layer must not be gold coated.

Diameter of 1st shield [m]	MLI outer layer	Test volume [K]	Optical bench [K]	Outer layer of 1st shield MLI [K]
0.9	Gold	11.4	24.5	123.4
2.4	Gold	9.7	18.9	520.5
2.4	Black	9.7	19.1	370.7

3.5.2. Extension of the shields

Can we improve the role of shields as radiators removing heat from struts and spacecraft to deep space by using larger shields? Let us assume shields just large enough to still fit into a Soyuz-Fregat fairing with 2.8 m diameter. The strut configuration and the dimensions of the interface with the spacecraft remain the same. The first shield extends beyond the spacecraft and receives direct solar radiation, which we model using the Monte-Carlo method (see Section 2.1). Extending the shields leads to a reduction of the TV and OB temperatures by 1.7 K and 5.5 K, respectively (see Table 1).

3.5.3. Heat-flow analysis for the optical bench

Fig. 9 shows the results of a heat-transfer analysis of the OB performed to identify possible design improvements. To improve the TV and OB temperatures, we investigated the gold coating on the OB. The area directly below the TV was gold coated ($\epsilon = 0.02$). The remaining surface area has $\epsilon = 0.80$. By increasing the gold-coated area, the bench top surface radiates less to deep space, increasing the overall OB temperature (from 23.1 K to 24.4 K) but decreasing the TV temperature (from 18.4 K to 11.1 K).

More detailed investigations of the technical requirements of MAQRO like decohering effects due to non-isotropic thermal radiation may allow further improving the ratio between gold-coated and uncoated areas of the OB.

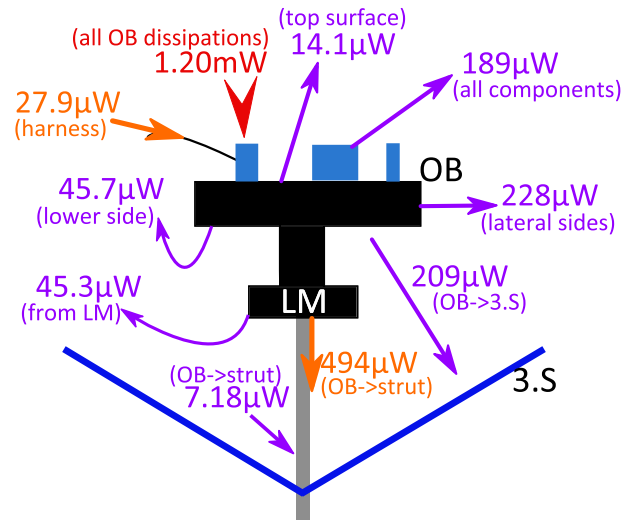


Fig. 9. Schematic heat-flow diagram of the optical bench. We divided the OB into lower and lateral surfaces, the LM and the optical components. The latter radiate a large part of heat to space because the OB dissipation is largely caused by the detector chip and the cavity mirrors. The OB top surface radiates little because of its gold finishing.

4. Conclusions

We investigated performance and design aspects of a radiatively cooled system for the proposed MAQRO mission. This instrument consists of an optical bench (OB) externally mounted to the spacecraft surface via three struts and shielded against direct heat exchange with the spacecraft and the sun. We implemented a geometric and a thermal mathematical instrument model using numerical tools like ESATAN-TMS and TransFAST.

A heat-flow analysis of the entire instrument shows that the shields block the spacecraft radiation and act as radiators, receiving heat from the instrument and emitting it to space. We showed that the instrument configuration using three shields thermally performs well, and that positioning the preprocessing chip for optical imaging below the first shield diverted the resulting dissipation heat into the shield rather than into the OB.

A transfer-function analysis showed that the shield structure strongly attenuates variations of the spacecraft temperature and of the preprocessing chip's dissipation. Considering a fluctuation period of 100 s, the fractional frequency instability of the cavity on the OB is comparable to the values achieved in ground-based cavities.

By a simple modification of the imaging optics on the OB we achieved a reduction from 13.9 K to 11.2 K for the test-volume (TV) temperature.

Analyzing orbital cases, we showed that, starting from 20 °C, it takes ~8 days for the TV and ~24 days for the OB to cool below 20 K in an L2 orbit. These times can be reduced significantly using SiC instead of ZERODUR® for the OB. For an HEO with a period of ~20 days, the time needed for cooling below the technical requirements of MAQRO significantly restricts the time for experiments to 11 days for each period for a ZERODUR® bench. This limitation is more relaxed for an SiC bench.

Extending the shields allows a temperature reduction from 11.4 K to 9.7 K and from 24.5 K to 19.1 K for TV and OB, respectively.

Acknowledgments

We acknowledge support from the Austrian Research Promotion Agency (FFG, Projects Nos. 840089 and 854036) and from the European Research Council (ERC) under the European Union's Horizon 2020 research and innovation programme (grant agreement No 649008).

References

- [1] Airbus DS GmbH, Claude-Dornier-Str., 88090 Immenstaad, Germany (Databank).
- [2] NIST Cryogenics Technologies Group. <http://cryogenics.nist.gov/MPropsMAY/5083%20Aluminum/5083Aluminum_rev.htm>.
- [3] C. Ho, M. Ackerman, K. Wu, S. Oh, T. Havill, *Phys. Chem. Ref. Data* 7 (3) (1978) 959.
- [4] G. Hartwig, S. Knaak, *Fibre-epoxy composites at low temperatures*, *Cryogenics* (1984) 644.
- [5] R. Reed, M. Golda, *Cryogenic properties of unidirectional composites*, *Cryogenics* (1994) 925.
- [6] V. Koshchenko, A. Demidenko, N. Prokofeva, V. Yachmenev, A. Radchenko, *Inorg. Mater. (USSR)* 15 (7) (1979) 1017.
- [7] V. Koshchenko, Y. Grinberg, R. Koschchenko, *Inorg. Mater. (USSR)* 21 (2) (1985) 197.
- [8] RMI Titanium Co, 1000 Warren Ave., Niles Ohio, 44446, USA and NIST, Physical and Chemical Properties Division, Cryogenics Technologies Group. <cryogenics.nist.gov>.
- [9] O. Umezawa, K. Ishikawa, *Cryogenics* 32 (10) (1992) 873.
- [10] H. Deem, W. Wood, C. Lucks, *Trans. Metall. Soc. AIME* 212 (1958) 520–523.
- [11] W. Ziegler, J. Mullins, Georgia Inst. Technology, Final Rept., Proj. No. A-504, 1961, pp. 1–54.
- [12] A. Cezairliyam, J. McClure, R. Taylor, *Res. Natl. Bureau Stand. A* 81A (2/3) (1997) 251.

- [13] C. Lucks, H. Thompson, A. Smith, F. Curry, H. Deem, G. Bing, USAFTR 6145 I, 1951, pp. 1–127 (ATI 117 715).
- [14] Department of Defense Handbook, *Metallic Materials and Elements for Aerospace Vehicles Structures*, MIL-HDBK-5J, 31 January 2003.
- [15] ZERODUR® Glaskeramik - schott ag, catalogue, 2004, pp. 8. <<http://www.schott.com/>>.
- [16] L. Hacker Müller, K. Hornberger, B. Brezger, A. Zeilinger, M. Arndt, *Decoherence of matter waves by thermal emission of radiation*, *Nature* 427 (2004) 711–714, <http://dx.doi.org/10.1038/nature02276>.
- [17] L. Hacker Müller, K. Hornberger, B. Brezger, A. Zeilinger, M. Arndt, *Decoherence in a Talbot Lau interferometer: the influence of molecular scattering*, *Appl. Phys. B* 77 (2003) 781–787, <http://dx.doi.org/10.1007/s00340-003-1312-6>.
- [18] O. Romero-Isart, A.C. Pflanzer, F. Blaser, R. Kaltenbaek, N. Kiesel, M. Aspelmeyer, J.I. Cirac, *Large quantum superpositions and interference of massive nanometer-sized objects*, *Phys. Rev. Lett.* 107 (2) (2011) 020405, <http://dx.doi.org/10.1103/PhysRevLett.107.020405>.
- [19] R. Kaltenbaek, G. Hechenblaikner, N. Kiesel, O. Romero-Isart, K.C. Schwab, U. Johann, M. Aspelmeyer, *Macroscopic quantum resonators (MAQRO) – testing quantum and gravitational physics with massive mechanical resonators*, *Exp. Astron.* 34 (2) (2012) 123–164, <http://dx.doi.org/10.1007/s10686-012-9292-3>.
- [20] B. Swinyard, T. Nakagawa, *The space infrared telescope for cosmology and astrophysics: SPICA A joint mission between JAXA and ESA*, *Exp. Astron.* 23 (1) (2009) 193–219, <http://dx.doi.org/10.1007/s10686-008-9090-0>.
- [21] T.G. Hawarden, R.O. Cummings, C.M. Telesco, H.A. Thronson Jr., *Optimised radiative cooling of infrared space telescopes and applications to possible missions*, *Space Sci. Rev.* 61 (1992) 113–144, <http://dx.doi.org/10.1007/BF0021248>.
- [22] T.G. Hawarden, R. Crane, H.A. Thronson Jr, A.J. Penny, A.H. Orlowska, T.W. Bradshaw, *Radiative and hybrid cooling of infrared space telescopes*, in: *Infrared and Submillimeter Space Missions in the Coming Decade*, Springer, 1996, pp. 45–56, <http://dx.doi.org/10.1007/BF00751251>.
- [23] P.A. Lightsey, C. Atkinson, M. Clampin, L.D. Feinberg, *James Webb Space Telescope: large deployable cryogenic telescope in space*, *Opt. Eng.* 51 (1) (2012) 011003-1, <http://dx.doi.org/10.1117/1.OE.51.1.011003>.
- [24] J. de Bruijne, *Science performance of Gaia, ESAs space-astrometry mission*, *Astrophys. Space Sci.* 341 (1) (2012) 31–41, <http://dx.doi.org/10.1007/s10509-012-1019-4>.
- [25] E. Urgoiti, G. Migliorero, *Mechanisms for GAIA deployable sunshield*, 11th European Space Mechanisms and Tribology Symposium, ESMATS 2005, vol. 591, 2005, pp. 163–170. <<http://www.esmats.eu/esmatspapers/pastpapers/pdfs/2005/urgoit1.pdf>>.
- [26] J.A. Tauber, N. Mandolesi, J.-L. Puget, et al., *Planck pre-launch status: The Planck mission*, *Astron. Astrophys.* 520 (2010) A1-1, <http://dx.doi.org/10.1051/0004-6361/200912983>.
- [27] W. Oran, R. Naumann, *Preliminary Assessment of the Vacuum Environment in the Wake of Large Space Vehicles*, NASA STI/Recon Technical Report N 77, 1977, pp. 31222.
- [28] R. Kaltenbaek, G. Hechenblaikner, N. Kiesel, F. Blaser, S. Gröblacher, S. Hofer, W. Vanner, M. R. Wiecek, K.C. Schwab, U. Johann, M. Aspelmeyer, *Macroscopic Quantum Experiments in Space Using Massive Mechanical Resonators*, Tech. Rep., Study Conducted Under Contract with the European Space Agency, Po P5401000400, 2011–2012.
- [29] G. Hechenblaikner, F. Hufgard, J. Burkhardt, N. Kiesel, U. Johann, M. Aspelmeyer, R. Kaltenbaek, *How cold can you get in space? Quantum physics at cryogenic temperatures in space*, *New J. Phys.* 16 (1) (2014) 013058, <http://dx.doi.org/10.1088/1367-2630/16/1/013058>.
- [30] P.J. Love, A.W. Hoffman, N.A. Lum, K.J. Ando, W.D. Ritchie, N.J. Therrien, A.G. Toth, R.S. Holcombe, *1 K × 1 K Si:As IBC detector arrays for JWST MIRI and other applications*, *Proc. SPIE* 5499 (2004) 86–96, <http://dx.doi.org/10.1117/12.555219>.
- [31] ITP Engines UK Ltd., *ESATAN-TMS Thermal Engineering Manual*, Tech. Rep., 2010. <www.esatan-tms.com>.
- [32] N. Kiesel, F. Blaser, U. Delic, D. Grass, R. Kaltenbaek, M. Aspelmeyer, *Cavity cooling of an optically levitated submicron particle*, *Proc. Natl. Acad. Sci. USA* 110 (35) (2013) 14180–14185, <http://dx.doi.org/10.1073/pnas.1309167110>.
- [33] R. Kaltenbaek, *Testing quantum physics in space using optically trapped nanospheres*, *Optical Trapping and Optical Micromanipulation X*, vol. 8810, 2013, p. 88100B, <http://dx.doi.org/10.1117/12.2027051>. Available from: 1307.7021.
- [34] P. McNamara, S. Vitale, K. Danzmann, on behalf of the LISA Pathfinder Science Working Team, *LISA Pathfinder*, *Classical Quant. Grav.* 25 (11) (2008) 114034, <http://dx.doi.org/10.1088/0264-9381/25/11/114034>.
- [35] E.J. Elliffe, J. Bogenstahl, A. Deshpande, J. Hough, C. Killow, S. Reid, D. Robertson, S. Rowan, H. Ward, G. Cagnoli, *Hydroxide-catalysis bonding for stable optical systems for space*, *Classical Quant. Grav.* 22 (10) (2005) 257–267, <http://dx.doi.org/10.1088/0264-9381/22/10/018>.
- [36] M. Williamson, *Spacecraft Technology: The Early Years*, The Institution of Engineering and Technology, 2006. <<https://books.google.com/books?id=np15NsFG8ngC&pgis=1>>.
- [37] J. Hanson, B. Beard, *Applying Monte Carlo Simulation to Launch Vehicle Design and Requirements Analysis*, National Aeronautics and Space Administration, Marshall Space Flight Center, 2010.
- [38] E. Zitzler, K. Deb, L. Thiele, *Comparison of multiobjective evolutionary algorithms: empirical results*, *Evol. Comput.* 8 (2) (2000) 173–195.
- [39] M. Loose, J. Beletic, J. Blackwell, J. Garnett, S. Wong, D. Hall, S. Jacobson, M. Rieke, G. Winters, *The SIDECAR ASIC: focal plane electronics on a single chip*,

- in: *Optics & Photonics*, International Society for Optics and Photonics, 2005 <http://dx.doi.org/10.1117/12.619638>. 59040V–59040V.
- [40] E. Messerschmid, S. Fasoulas, *Thermalkontrollsysteme*, in: *Raumfahrtssysteme*, Springer, Berlin, Heidelberg, 2011, pp. 333–370.
- [41] J. Crank, P. Nicolson, A practical method for numerical evaluation of solutions of partial differential equations of the heat-conducting type, *Math. Proc. Camb. Philos. Soc.* 43 (1) (1947) 50–67, <http://dx.doi.org/10.1007/BF02127704>.
- [42] L.F. Shampine, C.W. Gear, A user's view of solving stiff ordinary differential equations, *SIAM Rev.* 21 (1) (1979) 1–17, <http://dx.doi.org/10.1137/1021001>.
- [43] M. Altenburg, J. Burkhardt, *Application of Linear Control Methods to Satellite Thermal Analysis*, Tech. Rep., ICES 2008-01-2076, San Francisco, June 2008. <http://dx.doi.org/10.4271/2008-01-2076>.
- [44] M. Altenburg, J. Burkhardt, *Advances in frequency domain thermal analysis based on linearized thermal networks*, in: 24th European Workshop on Thermal and ECLS Software, ESTEC, Noordwijk, The Netherlands, 2010. <<https://exchange.esa.int/thermal-workshop>>.
- [45] SRE-PA & D-TEC Staff, *Margin Philosophy for Science Assessment Studies*, Tech. Rep., ESA/ESTEC, Noordwijk, 2012. <sci.esa.int/science-e/www/object/doc.cfm?fobjectid=55027>.
- [46] K. Numata, A. Kemery, J. Camp, Thermal-noise limit in the frequency stabilization of lasers with rigid cavities, *Phys. Rev. Lett.* 93 (25) (2004) 250602, <http://dx.doi.org/10.1103/PhysRevLett.93.250602>.
- [47] M. Notcutt, L.-S. Ma, A.D. Ludlow, S.M. Foreman, J. Ye, J.L. Hall, Contribution of thermal noise to frequency stability of rigid optical cavity via Hertz-linewidth lasers, *Phys. Rev. A* 73 (3) (2006) 031804, <http://dx.doi.org/10.1103/PhysRevA.73.031804>.
- [48] S. Amairi, T. Legero, T. Kessler, U. Sterr, J.B. Wübbena, O. Mandel, P.O. Schmidt, Reducing the effect of thermal noise in optical cavities, *Appl. Phys. B* 113 (2) (2013) 233–242, <http://dx.doi.org/10.1007/s00340-013-5464-8>.
- [49] D. Gwo, *Hydroxide-catalyzed Bonding*, US Patent 6,548,176, 2003. <<http://www.google.com/patents/US6548176>>.
- [50] S. Roose, S. Heltzel, *High-precision Measurements of the Thermal Expansion at Cryogenic Temperature on Stable Materials*, Tech. Rep., Physikalisch-Technische Bundesanstalt (PTB), 2013. <http://dx.doi.org/10.7795/810.20130822T>.